Chee, Kuan W. A.; Tang, Ziqiang; Lü, Hong; Huang, Feng

Article

Anti-reflective structures for photovoltaics: Numerical and experimental design

Energy Reports

Provided in Cooperation with:
Elsevier

Suggested Citation: Chee, Kuan W. A.; Tang, Ziqiang; Lü, Hong; Huang, Feng (2018) : Anti-reflective structures for photovoltaics: Numerical and experimental design, Energy Reports, ISSN 2352-4847, Elsevier, Amsterdam, Vol. 4, pp. 266-273, https://doi.org/10.1016/j.egyr.2018.02.002

Energy Reports 4 (2018) 266–273

Contents lists available at ScienceDirect

Energy Reports

journal homepage: www.elsevier.com/locate/egyr

Research paper

Anti-reflective structures for photovoltaics: Numerical and experimental design

Kuan W.A. Chee [a,c,*], Ziqiang Tang [b], Hong Lü [a,d], Feng Huang [c]

[a] Department of Electrical and Electronic Engineering, Faculty of Science and Engineering, University of Nottingham Ningbo China, Ningbo 315100, China
[b] Department of Electrical and Computer Engineering, Faculty of Applied Sciences, University of British Columbia, Vancouver, BC, Canada V6T 1Z4
[c] Key Laboratory of Marine Materials and Related Technologies, Zhejiang Key Laboratory of Marine Materials and Protective Technologies, Ningbo Institute of Materials Technology and Engineering, Chinese Academy of Sciences, Ningbo, 315201, China
[d] Yisci Bio Co. Ltd., 3377 Kangxin Gonglu, Pudong District, Shanghai, 200120, China

ARTICLE INFO

Article history:
Received 29 October 2017
Received in revised form 24 February 2018
Accepted 24 February 2018

Keywords:
Photovoltaic cells
Surface engineering
Energy conversion
Thin films
Reflectivity

ABSTRACT

The effects of different anti-reflective structures on the photovoltaic performance of the silicon solar cell were studied using finite-element modelling and numerical simulations for which experiment alone does not provide a full description. The front surface reflectivity may be mitigated significantly by an anti-reflective coating (ARC) of a suitable thickness. Alternatively, nanoscale surface texturing can effectively trap a greater ratio of incident light to increase optical absorption. The optimized layer thicknesses of the ZnO single layer and SiO_2/Si_3N_4 double layer films were calculated for minimum reflectivity, with the former grown by magnetron sputter deposition and characterized using specular X-ray reflectivity measurements. Based on geometric ray-tracing and solutions to the semiconductor equations, the theoretical photovoltaic performance was simulated and compared for a range of incident angles at an optical intensity of 0.1 Wcm^{-2}, revealing a limit to the angular collection efficiency of the ARC at a grazing incidence angle of 30°. Using ZnO or SiO_2/Si_3N_4 ARCs or surface texturing increases the power conversion efficiency by 20%, 24% and 30% respectively at normal incidence. The insights provided by physical-based modelling on the optimized design parameters of the anti-reflective structures confer a promising pathway for enhancing the external quantum efficiency of photovoltaic devices.

1. Introduction

Over the past decade, the real price of electricity around the world has largely risen significantly, eg. by 63% in the U.K. (OVO Energy, 2018) or at 3% each year in U.S.A. (EnergySage, 2017a, b), partly driven by energy shortages owing to reliance on fossil fuels. On the contrary, the price of crystalline silicon photovoltaic panels has plummeted dramatically from $74 per watt in the early-1970s to less than 70 ¢ per watt in 2014 (Brown et al., 2015), and continuing to exhibit trends consistent with Swanson's law to date. Besides, solar energy delivers environmental benefits; the Solar Energy Industries Association reported that current levels of solar photovoltaic installation in the U.S.A. offset 37 million metric tons of carbon emissions (equivalent to planting 956 million trees) each year (EcoWatch, 2016), and the U.S. Environmental Protection Agency avers that carbon emissions can be slashed by 3 to 4 tons annually per two-person household by installing a solar power system (EnergySage, 2017a, b). Therefore the perceived socio-economic and environmental impacts continue to inspire the long-standing interest in harnessing sunlight to generate clean and sustainable electricity, with photovoltaic devices based on crystalline silicon wafers being the dominant technology in the solar energy market.

However, the power conversion efficiency (PCE) of crystalline solar cells is generally limited by the reflection of light at the surface, charge recombination and trapping in the material, energy dissipation caused by the cell's resistance, and temperature (Chanta et al., 2015; Filipowski et al., 2017; Chen and Shao, 2011; Cuce et al., 2013; Chander et al., 2015a, b). For bare or polished silicon, a significant fraction of the optical losses is due to the high index contrast resulting in a high surface reflection of nearly 35% over the complete AM1.5G spectrum. An approach to enhance optical absorption is therefore to design the front surface with anti-reflective structures that reduce reflection losses and enable increased photogeneration in the cell. The majority of the world's commercial silicon photovoltaics have so far relied on using single layer TiO_2, Si_3N_4 or SiO_2, but we explore ZnO single layer

* Corresponding author at: Department of Electrical and Electronic Engineering, Faculty of Science and Engineering, University of Nottingham Ningbo China, Ningbo 315100, China.
E-mail address: kuan.chee@nottingham.edu.cn (K.W.A. Chee).

https://doi.org/10.1016/j.egyr.2018.02.002

anti-reflective coating (SLARC) and SiO_2/Si_3N_4 double layer anti-reflective coating (DLARC) and benchmark with surface texturing. An anti-reflective coating (ARC) of transparent conducting oxide or dielectric material such as ZnO or SiO_2/Si_3N_4 thin films, when fabricated on the surface with an appropriate refractive index and film thickness, not only increases the short circuit current density through optical absorption and photogeneration, but like the ITO on SiO_2 (Drabczyk et al., 2016) or SiN_x:H (Kluska and Panek, 2016) layers, can passivate recombination sites and increase the open circuit voltage and fill factor. Specifically, the ZnO thin film is non-toxic and versatile, having high radiation tolerance at high temperature, is transparent in the visible region (Godlewski et al., 2009), and its synthesis relates to an established industry standard fabrication process. As a result, ZnO ARCs show a lot of promise for adoption in new technology solar cells. Without an expensive thermal budget, an experimental SLARC of ZnO was grown to an optimized thickness by RF magnetron sputter deposition on the crystalline silicon solar cell, and the layer thickness was measured using a specular X-ray reflectivity (XRR) technique. The emergent SiO_2/Si_3N_4 double layer thin film is known for its broadband transmissivity, which bestows a high absorption rate at shorter wavelengths. Furthermore, crystalline silicon surface texturing at the micro-/nano-scale can be applied to increase light trapping. In this paper, the effectiveness of the aforementioned anti-reflective structures will be investigated and compared by numerical simulations, which can provide valuable insights into the ideal design parameters. The results show that the PCE could be increased by up to 30% relative to that of the bare silicon solar cell for light incident normally on the surface.

2. Simulation and experimental methods

The two-dimensional finite-element models of the relevant cell structures (see Fig. 1) for SLARC, DLARC and surface texturing atop the silicon substrate were constructed and optimized. Arbitrary topologies, internal and external reflections and refractions, as well as polarization dependencies and dispersions, are accounted for by the TCAD software tool (Silvaco co.) to obtain exact solutions for general optical sources. In tandem with modelling optoelectronic interactions using geometric ray tracing, radiative, Shockley–Read–Hall and Auger recombinations in the bulk and surface were accounted for, plus energy balance and a range of other important (photo)physical device phenomena for photovoltaic cells; high-performance computation was carried out to obtain numerical solutions to the system of partial differential equations forming the basic semiconductor equations together with appropriate boundary conditions so that current–voltage characteristics, photogeneration rate, spectral response, etc., can be simulated (Michael and Bates, 2005). To allow meaningful comparison, identical device parameters were used, although most of them with conservative values. The SLARC is designed so that the relative phase shift between the beam specularly reflected at the upper and lower boundaries of the thin film is 180°. These two reflected beams will be cancelled by destructive interference before they exit the surface.

The required thickness of the ARC layer is given by:

$$t = \frac{\lambda}{4n_1} \tag{1}$$

where t is thickness, λ the free-space wavelength, and n_1, the index of refraction of the thin film ARC needed for complete cancellation of the two beams is given by Swatowska et al. (2011):

$$n_1 = \sqrt{(n_0 n_s)};\ (n_s > n_1) \tag{2}$$

where n_0 is the index of refraction of air (or the incident material) and n_s is the index of refraction of the substrate. n_s should be

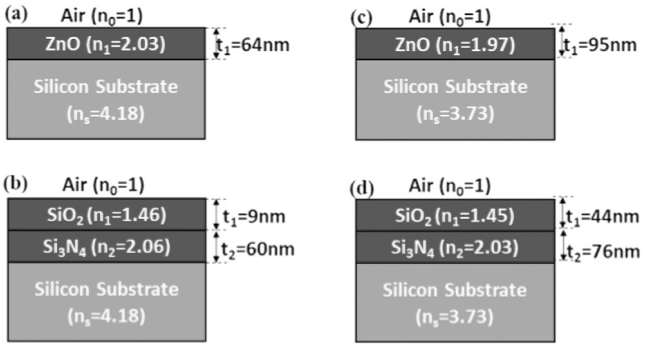

Fig. 1. Solar cell structures with (a) ZnO SLARC and (b) SiO_2/Si_3N_4DLARC at an incident wavelength of 525 nm, and (c) ZnO SLARC and (d) SiO_2/Si_3N_4DLARC at an incident wavelength of 750 nm.

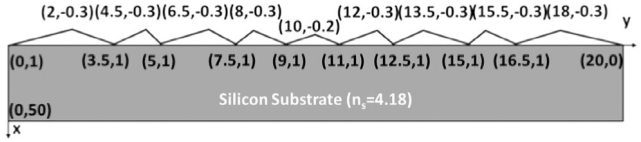

Fig. 2. Schematic of surface texturing (not to scale). The coordinates are in units of microns.

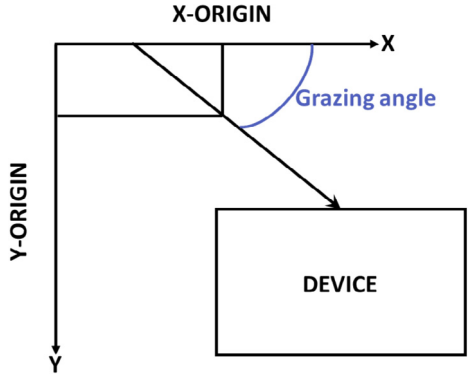

Fig. 3. Optical beam geometry.

greater than n_1 to maintain the optical effectiveness of the ARC layer (Zoolfakar, 2009). To achieve zero reflectance in DLARCs, the thickness of each layer must satisfy (Ali et al., 2014):

$$t_1 = \frac{\lambda}{2\pi n_1} tan^{-1}\left\{\pm\left[\frac{(n_s - n_0)\left(n_s n_0 - {n_2}^2\right){n_1}^2}{\left(n_s {n_1}^2 - n_0 {n_2}^2\right)\left({n_1}^2 - n_s n_0\right)}\right]\right\}$$
$$t_2 = \frac{\lambda}{2\pi n_2} tan^{-1}\left\{\pm\left[\frac{(n_s - n_0)\left(n_s n_0 - {n_1}^2\right){n_2}^2}{\left(n_s {n_1}^2 - n_0 {n_2}^2\right)\left({n_2}^2 - n_s n_0\right)}\right]\right\} \tag{3}$$

where t_1 and t_2 are the optimal thicknesses, and n_1 and n_2 are the refractive indices of the top and bottom layers respectively.

Any reflected light can scatter repeatedly on a textured silicon surface, thus enhancing the absorption ratio. The coordinates of the triangular mesh rendering an arbitrarily textured surface was defined as shown in Fig. 2.

The grazing angle (propagation of the beam relative to the surface plane) is defined by parameter ANGLE (see Fig. 3). For example, ANGLE = 90 means the illumination is perpendicular to the surface. The design parameters used for the solar cell performance simulations is listed in Table 1.

Table 1
Parameters for solar cell simulation.

No.	Name of parameter	Value
1	Optical intensity	0.1 Wcm^{-2}
2	Silicon sample length	20 μm
3	Silicon sample width	1 μm
4	P-type background doping concentration	$1 \times 10^{14} cm^{-3}$
5	N-type background doping concentration	$1 \times 10^{15} cm^{-3}$
6	Junction depth	0.25 μm
7	Diffusion temperature	900 K
8	Auger lifetime for electrons	1 μs
9	Auger lifetime for holes	1 μs
10	Cathode material	Aluminium
11	Cathode thickness	0.1 μm
12	Primary light source	AM1.5D spectrum (National Renewable Energy Laboratory, 2017)
13	Wavelength range	300 through 1000 nm
14	Refractive index of ZnO	2.03 (Polyanskiy, 2017) (525 nm),1.97 (Polyanskiy, 2017) (750 nm)
15	Refractive index of SiO_2/Si_3N_4	1.46 (Polyanskiy, 2017) (525 nm)/2.06 (Polyanskiy, 2017) (525 nm) 1.45 (Polyanskiy, 2017) (750 nm)/2.03 (Polyanskiy, 2017) (750 nm)

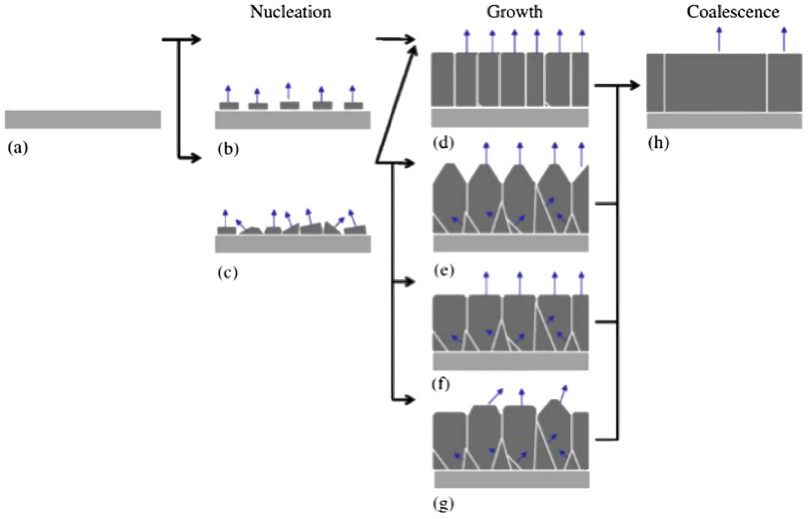

Fig. 4. Schematic process diagram illustrating stages of polycrystalline film deposition (reproduced with permission from Kajikawa (2006)). (a) Preparation of the thin film substrate, (b) initial nuclei with PO according to the surface energy of epitaxial substrate, (c) initial nuclei exhibiting random orientation on non-epitaxial substrate, (d) equiaxed columnar, (e) non-equiaxed columnar and textured surface, (f) non-equiaxed columnar without surface texture, (g) non-equiaxed columnar without PO, and (h) columnar. PO processes are preferential nucleation and ripening (a → b), initial grain growth (c → d), surface diffusion on non-textured surface and sticking (c → e), surface diffusion among grains (c → f), and grain growth (d, e, f, g–h).

The ZnO SLARC was grown by RF magnetron sputter deposition under a base pressure of 0.7 Pa at room temperature. Fig. 4 illustrates the evolution of surface texture during thin polycrystalline ZnO film deposition. In the nucleation phase, the ZnO nuclei were formed on the SiO_2 surface layer of the substrate (see Fig. 4(a), (b) and (c)). The nucleation was initiated either with a preferred orientation (PO) normal to the substrate or random orientation. Thereafter, the film texture becomes equiaxed columnar if the initial nuclei has PO (see Fig. 4(d)), or if random orientation of the nuclei were initialized (see Fig. 4(c)), the interim grain orientations will be dominated by the fastest growth direction normal to the substrate (see Fig. 4(e) and (f)), ultimately leading to coalescence and PO (see Fig. 4(h)).

The layer thickness of the SLARC was measured by non-destructive XRR using the Bruker D8 HRXRD. The positions of interference fringes originating from multiple reflections of the X-rays at the film/substrate interface in a specular reflectivity scan can provide precise determination (within 1% or less) of the thickness value. The modified Bragg equation used to analyse the raw data is (Huang et al., 2002; Azaroff, 1968):

$$\sin^2\theta_m = {\theta_c}^2 + (m + \Delta m)^2\left(\frac{\lambda}{2t}\right)^2 \tag{4}$$

where m is an integer indicating the reflection order, θ_m is the observed angular position corresponding to the maxima or minima of the m^{th} interference fringe ($\Delta m = 0.5$ for the intensity maximum and $\Delta m = 0$ for the intensity minimum), θ_c is critical angle for total internal reflection, and λ is the X-ray wavelength. Since Eq. (4) can be represented as a linear function in the form $y = kx + b$ [where the slope k is $\left(\frac{\lambda}{2t}\right)^2$], the film thickness t can be determined from:

$$t = \frac{\lambda}{2\sqrt{k}} \tag{5}$$

3. Results and discussion

3.1. Optimized ARC layer thickness

The simulation results indicate that the optimized thicknesses of the ZnO SLARC are 64 nm and 95 nm at a wavelength of 525 and 750 nm respectively, while those of the SiO_2/Si_3N_4 DLARC are 9 nm/60 nm and 44 nm/76 nm at a wavelength of 525 and 750 nm respectively. Fig. 5 compares the reflectivity with and without ARCs at the incident wavelengths of 525 and 750 nm. It can be clearly seen that the reflectivity is significantly mitigated at their designed wavelengths. The minimum reflectivity corresponds to

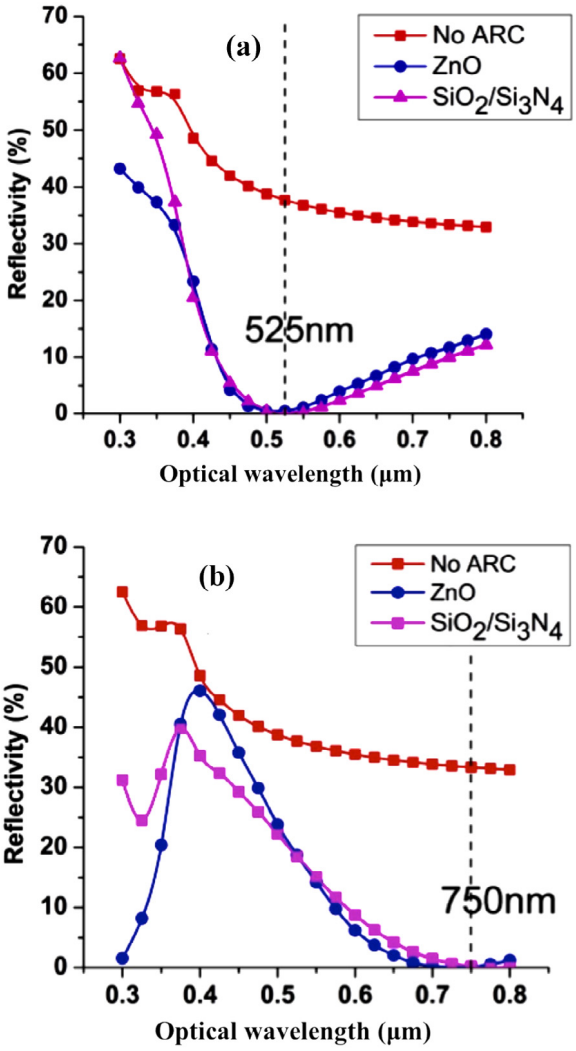

Fig. 5. Reflectivity versus optical wavelength for an optimized ZnO SLARC (SiO_2/Si_3N_4 DLARC) thickness of (a) 64 nm (9 nm/60 nm) and (b) 95 nm (44 nm/76 nm).

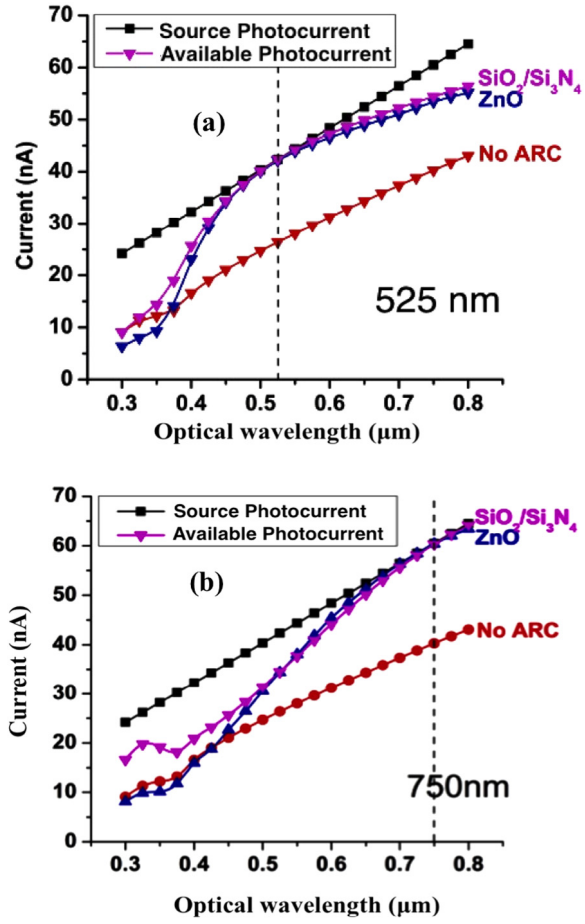

Fig. 6. Source and available photocurrent versus optical wavelength for an optimized ZnO SLARC (SiO_2/Si_3N_4 DLARC) thickness of (a) 64 nm (9 nm/60 nm) and (b) 95 nm (44 nm/76 nm).

the respective wavelengths at which the combination of thickness and refractive index facilitates destructive interference between the anti-phase reflected waves from the top (with air) and bottom (with silicon) interfaces of the ARC layer.

Fig. 6 depicts the frequency-dependent source photocurrent (available in the light beam) and available photocurrent (generated by optical absorption) with and without ARCs. The results show that more photocurrent can be generated in the solar cell with an ARC, whereas superior photoelectric performance can be achieved using SiO_2/Si_3N_4DLARC especially for shorter wavelengths. With the aid of the ZnO SLARC and SiO_2/Si_3N_4DLARC designs, the external quantum efficiency (EQE), which can be evaluated from the ratio of the respective photocurrents (Zoolfakar, 2009):

$$EQE = \frac{I_{available\ \text{photocurrent}}}{I_{source\ \text{photocurrent}}} \tag{6}$$

can be increased by 49.1% and 49.8% respectively at an incident wavelength of 525 nm (see Fig. 7).

Fig. 8(a) shows an XRR pattern at grazing incidence of a ZnO SLARC film sputter deposited on the silicon solar cell, which is characterized by reflectivity oscillations with positions and spacings of the interference fringes allowing direct determination of the lamella thickness. The least squares regression of the data consisting of well-defined maxima and minima of the specular reflectivity curve is shown in Fig. 8(b), which from the modified Bragg formalism (see Eq. (4)) provides for a slope of $8.695 \times 10^{-7}\,m^{-2}$, an estimated thickness of 58 nm (Eq. (5)), which is nearly the optimized thickness for an incident wavelength of 525 nm.

3.2. Grazing angle dependence of photovoltaic performance

Fig. 9 shows the photogeneration profiles in the photovoltaic cell with and without ARC under different angles of illumination at an incident wavelength of 525 nm. At non-normal incidence, the ray-tracing inside the device corresponding to refraction effects can be observed. The photogeneration rate increases with the grazing angle as beam propagation and optical absorption deep into the bulk of the cell is maximized, therefore in turn increasing the photogenerated current. Conversely, the photogeneration rate reduces with grazing angle as the beam propagates a greater distance along the surface, thereby contributing little to the quantum efficiency with a larger fraction of the optical beam being reflected back out of the cell.

Hence, the photogeneration rate is a critical parameter to justify the solar cell's PCE, which is calculated by:

$$PCE = \frac{P_{max}}{P_{in}} = \frac{(V_{oc}J_{sc})FF}{P_{in}} \tag{7}$$

where J_{SC} is the short-circuit current density, V_{oc} is the open circuit voltage, FF is the fill factor (ratio of maximum output power density P_{max} to $V_{oc} \times J_{sc}$) and P_{in} is the solar irradiance.

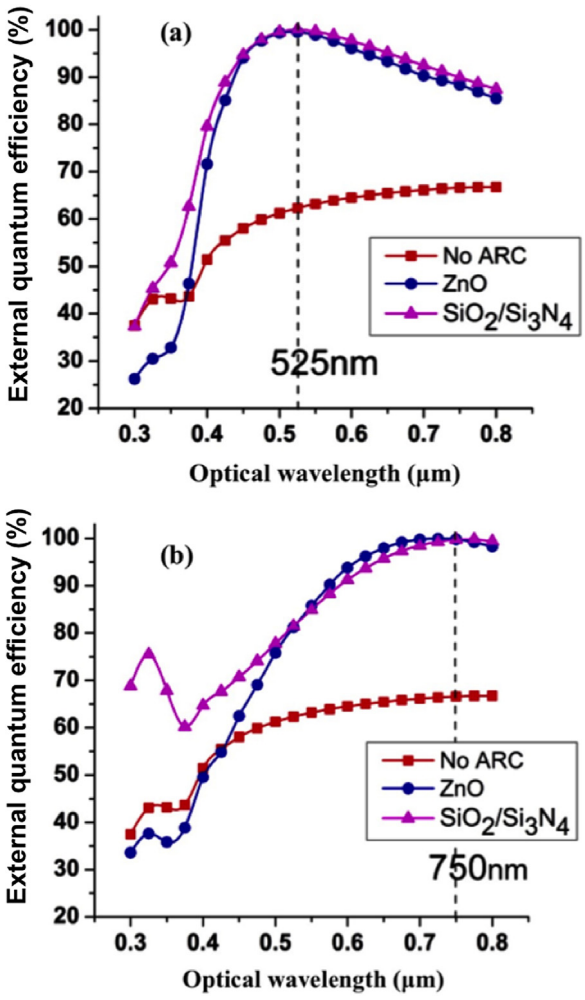

Fig. 7. External quantum efficiency versus optical wavelength for an optimized ZnO SLARC (SiO_2/Si_3N_4 DLARC) thickness of (a) 64 nm (9 nm/60 nm) and (b) 95 nm (44 nm/76 nm).

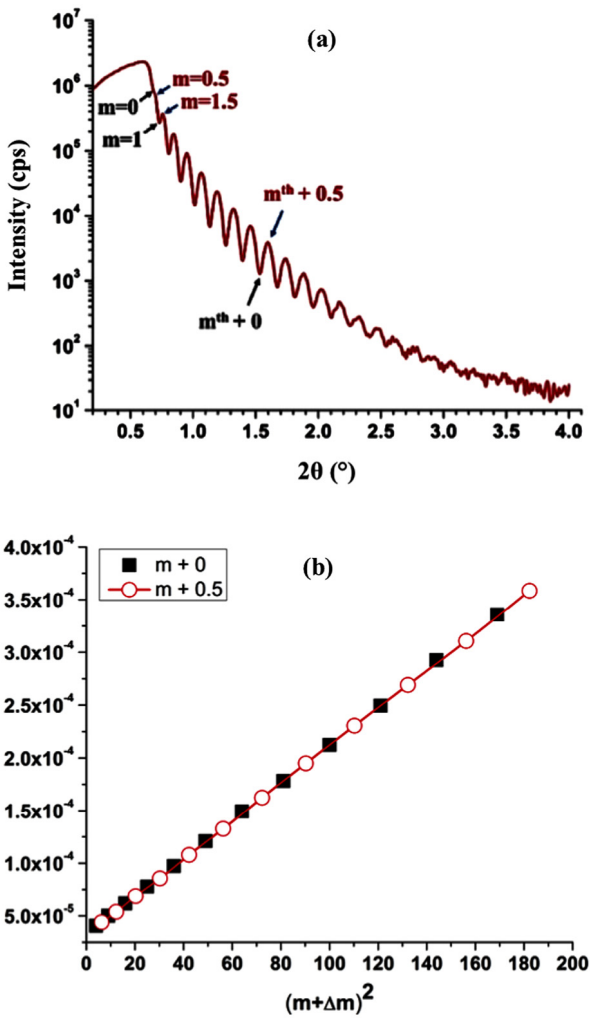

Fig. 8. (a) A representative specular XRR curve from the ZnO film on an SiO_2 substrate, and (b) $\sin^2\theta_m$ versus $(m + \Delta m)^2$ plot for the maxima and minima of the well-defined interference fringes.

The current–voltage characteristic curves at wavelengths 300 through 1000 nm are shown in Fig. 10, indicating increased optical losses via Fresnel effects as the grazing angle of illumination reduces. The Table 2 results demonstrate that the PCE increases with grazing angle, reaching a maximum at normal incidence. Moreover, it is clear that light trapping and optical absorption is generally enhanced when designed with ARCs, as revealed in the increased photogenerated current (see Fig. 10), so that the solar cell exhibits superior PCE (see Table 2). With more effective suppression of reflectance by the ARC, the SiO_2/Si_3N_4 DLARC design permits the highest PCE amongst these three types of solar cells with 6.2%, 5.6% and 3.4% at the grazing angles of 90°, 60°and 30° respectively. The diminishing difference in PCE values between the coated and uncoated solar cells as the grazing angle decreases to 30° indicates the angular collection efficiency limits of the ARCs studied.

Table 2
Photovoltaic parameters and calculated efficiency values.

Grazing angle	J_{sc} (mA/cm^2)	V_{oc} (mV)	FF	PCE (%)
		Bare solar cell		
30°	11.34	390	0.750	3.32
60°	15.68	397	0.751	4.67
90°	16.74	399	0.751	5.01
		ZnO-coated solar cell		
30°	11.49	390	0.750	3.36
60°	18.11	401	0.752	5.46
90°	20.12	403	0.752	6.01
		SiO_2/Si_3N_4-coated solar cell		
30°	11.64	390	0.750	3.41
60°	18.43	401	0.752	5.56
90°	20.42	404	0.752	6.20

3.3. Surface texturing effects on solar cell performance

Besides inducing a plurality of surface reflections, random texturing creates the effect of increasing the grazing angle to the surface of the optical beam incidence, hence increasing light trapping efficiency. The photovoltaic performance advantage due to surface texturing is compared with those using ARCs atop planar surfaces at an incident wavelength of 525 nm. Fig. 11 illustrates the photogeneration rate within the textured silicon solar cell for an optical beam incident normally on the top surface. Unlike that shown in Fig. 9(a) for a bare planar surface, the photogeneration rate directly beneath the aluminium contact is highest as the light collection solid angle is enlarged, thereby accounting for the 30% increase in PCE (see Table 3). It is conceivable that the solar irradiation impinging on the textured surface experiences multiple reflections, and is partially absorbed at each reflection, thereby minimizing the directional hemispherical reflectance.

The current–voltage characteristic curves in Fig. 12(a) illustrate the increased photogenerated current for the textured solar cell

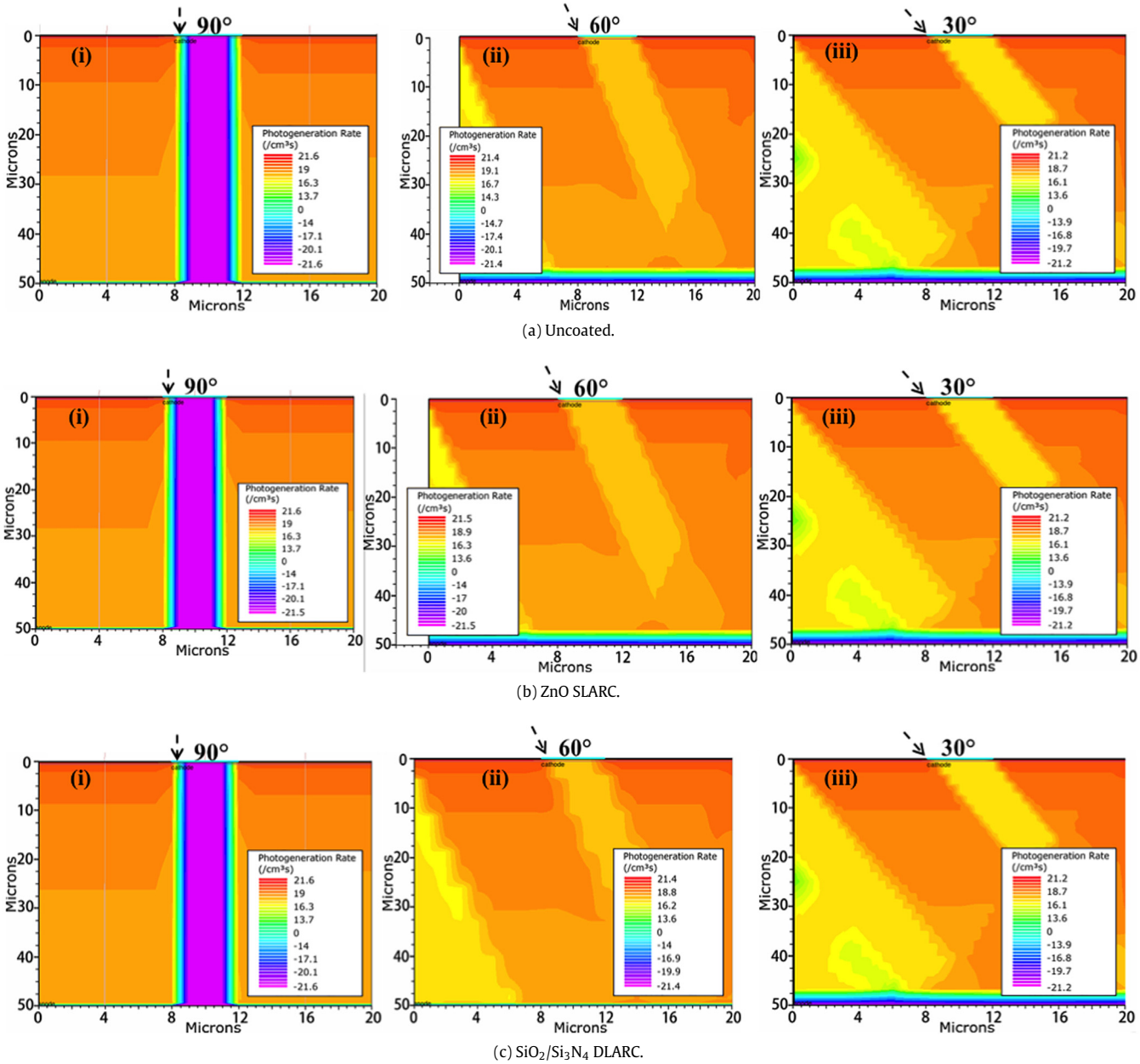

Fig. 9. Photogeneration rate in silicon solar cell, (a) uncoated, or coated with a (b) ZnO SLARC or (c) SiO_2/Si_3N_4 DLARC atop the silicon substrate, under optical illumination at (i) normal incidence, or at a grazing incidence angle of (ii) 60°or (iii) 30°.

resulting from enhanced light trapping and optical absorption in the substrate. The photovoltaic performance parameters are summarized in Table 3, which denote the importance of ARC structures in boosting the power output, and confirming that the textured surface provides the highest PCE in this study. The amount of available photocurrent as a function of optical wavelength for the range of specimens shows that surface texturing is able to outperform that of the other designs in the visible to near infrared wavelength range from 650 through 1000 nm (Fig. 12(b)).

Table 3
Photovoltaic parameters and calculated efficiency values.

Type	J_{sc} (mA/cm^2)	V_{oc} (mV)	FF	PCE (%)
Bare cell	16.73	399	0.7512	5.01
ZnO SLARC cell	20.12	403	0.7522	6.10
SiO_2/Si_3N_4 DLARC cell	20.42	404	0.7522	6.21
Textured surface cell	21.36	404	0.7527	6.50

4. Conclusion

In the present study, the optical performance enhancement conferred by the ZnO SLARC, SiO_2/Si_3N_4 DLARC and surface texturing on the silicon solar cell was investigated and compared by finite-element modelling and numerical simulations. The optimized thickness of the ARC layer is a function of wavelength, which for ZnO SLARC is 64 nm and 95 nm at an incident wavelength of 525 nm and 750 nm respectively; and for SiO_2/Si_3N_4 DLARC is 9 nm/60 nm and 44 nm/76 nm for a wavelength of 525 nm and 750 nm respectively. An optimized thickness of the thin polycrystalline film of ZnO SLARC was grown on the oxidized silicon substrate, and a layer thickness of about 58 nm was measured using a specular XRR technique. The photogeneration rate as well as the PCE increase with the grazing angle, and become maximum at

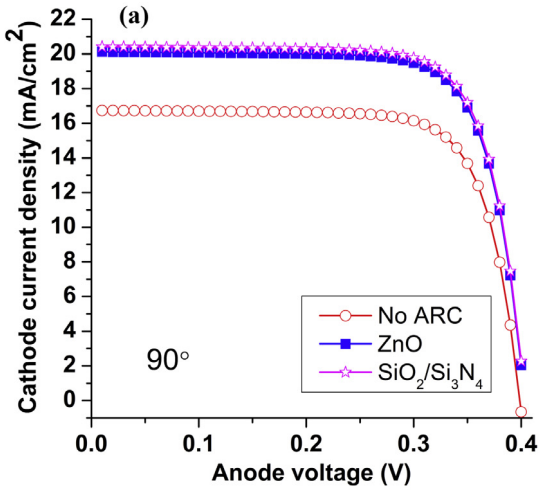

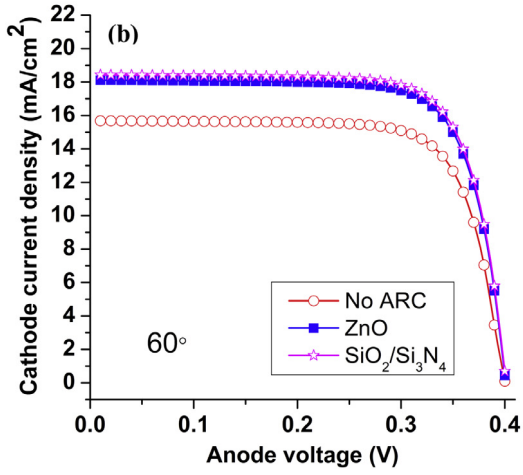

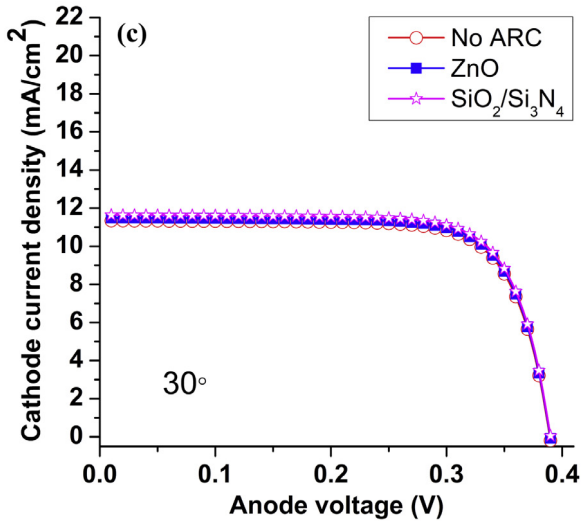

Fig. 10. Current–voltage characteristic curves with optical illumination at (a) normal incidence, and at a grazing angle of (b) 60°and (c) 30°.

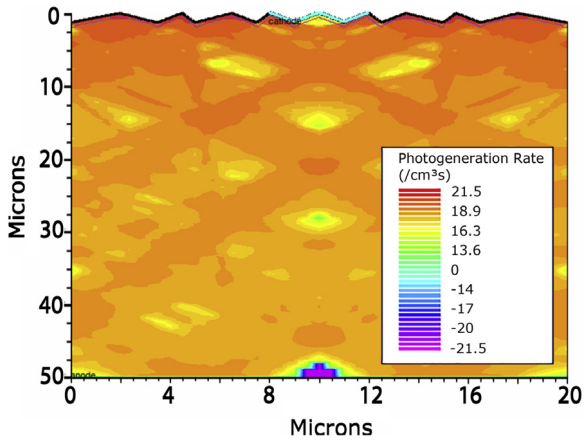

Fig. 11. Photogeneration contours due to optical illumination and absorption in silicon solar cell with textured surface.

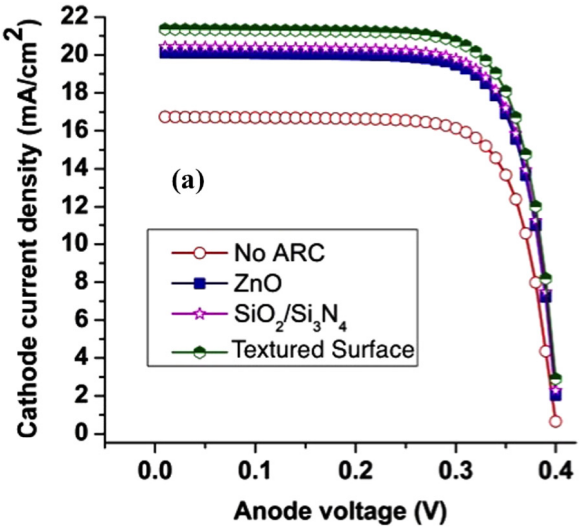

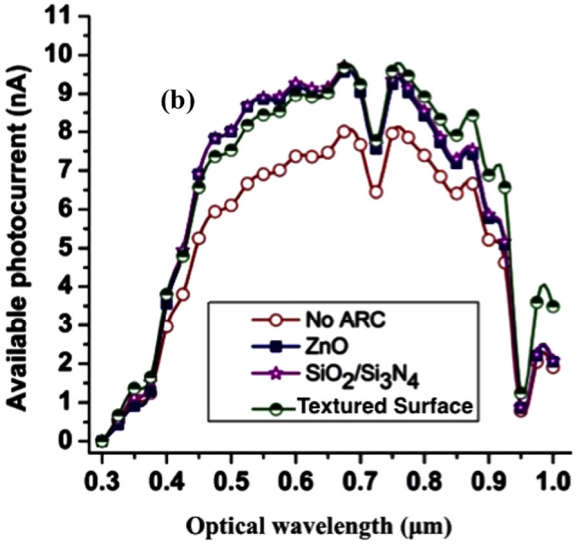

Fig. 12. (a) Current–voltage characteristic curves with optical illumination at normal incidence for silicon solar cell with and without anti-reflective structure, and (b) available photocurrent versus optical wavelength.

normal incidence. Notably, the PCE for bare silicon, ZnO SLARC, and SiO_2/Si_3N_4 DLARC solar cells is almost equivalent at a grazing angle of 30°, indicating the angular collection efficiency limit of the ARC. The current–voltage characteristics reveal that ARC and surface texturing significantly increase short-circuit current; and generally more photocurrent can be generated by using SiO_2/Si_3N_4 DLARC compared to ZnO SLARC. However, surface texturing provides the highest PCE (6.50%) compared to SiO_2/Si_3N_4 DLARC (6.21%) and

ZnO SLARC (6.10%), owing mainly to superior response characteristics in the near infrared regime. Taken together, this study has provided insights into the superior performance of the solar cell when using ARC and/or surface texturing, and demonstrated a protocol for the fabrication and characterization of an ARC.

Acknowledgements

The following grants are acknowledged: project No. 61650110517 supported by the Natural Science Foundation of China, project No. 2014A610154 and No. 2017A610095 supported by Ningbo Natural Science Foundation, and the "Hundred Talents Program" of the Chinese Academy of Sciences.

References

Ali, K., et al., 2014. Effect of double layer (SiO_2/TiO_2) anti-reflective coating on silicon solar cells. Int. J. Electrochem. Sci. 9, 7865–7874.

Azaroff, L.V., 1968. Elements of X-ray Crystallography, first ed. McGraw-Hill, New York.

Brown, L.R., et al., 2015. The Great Transition: Shifting from Fossil Fuels to Solar and Wind Energy, first ed. W.W. Norton & Company, New York.

Chander, S., et al., 2015a. Impact of temperature on performance of series and parallel connected mono-crystalline silicon solar cells. Energy Rep. 1, 175–180.

Chander, S., et al., 2015b. A study on photovoltaic parameters of mono-crystalline silicon solar cell with cell temperature. Energy Rep. 1, 104–109.

Chanta, E.S., et al., 2015. Effect of ZnO double layer as anti-reflection coating layer in ZnO dye-sensitized solar cells. In: 2015 International Conference on Alternative Energy in Developing Countries and Emerging Economies, Energy Procedia 79, 879–884.

Chen, A., Shao, Q., 2011. Simulation of high conversion efficiency and open-circuit voltages of α-si/poly-silicon solar cell. Sci. China Phys. Mech. Astron. 54, 1466–1470.

Cuce, E., et al., 2013. An experimental analysis of illumination intensity and temperature dependency of photovoltaic cell parameters. Appl. Energy 111, 374–382.

Drabczyk, K., et al., 2016. Influence of ITO layer application on electrical parameters of silicon solar cells with screen printed front electrode. Microelectron. Int. 33 (3), 172–175.

EcoWatch, 2016. Solar industry experiences record-breaking growth. https://www.ecowatch.com/solar-energy-record-growth-2003130851.html. (Accessed 22 February 2018).

EnergySage, 2017a. Renewable solar energy. https://www.energysage.com/solar/why-go-solar/protect-the-environment. (Accessed 3 April 2017).

EnergySage, 2017b. Why go solar –Top 10 benefits of solar energy. https://www.energysage.com/solar/why-go-solar/. (Accessed 3 April 2017).

Filipowski, W., et al., 2017. Spray-on glass solution for fabrication silicon solar cell emitter layer. Microelectron. Int. 34 (3), 149–153.

Godlewski, M., et al., 2009. ZnO layers grown by atomic layer deposition: A new material for transparent conductive oxide. Thin Solid Films 518 (4), 1145–1148.

Huang, F., et al., 2002. Room-temperature oxidation of ultrathin TiB_2 films. J. Mater. Res. 17 (4), 805–813.

Kajikawa, Y., 2006. Texture development of non-epitaxial polycrystalline ZnO films. J. Crystal Growth 289 (1), 387–394.

Kluska, S., Panek, P., 2016. Influence of the SiN_x:H layer deposited by PECVD technique on the surface and grain boundary passivation of mc-Si. Microelectron. Int. 33 (3), 162–166.

Michael, S., Bates, A., 2005. The design and optimization of multijunction solar cells using the Silvaco ATLAS software package. Sol. Energy Mater. Sol. Cells 87, 785–794.

National Renewable Energy Laboratory, 2017. Reference Solar Spectral Irradiance: Air Mass 1.5. http://rredc.nrel.gov/solar/spectra/am1.5/. (Accessed 3 April 2017).

OVO Energy, 2018. Average electricity prices around the world: $/kW. https://www.ovoenergy.com/guides/energy-guides/average-electricity-prices-kwh.html. (Accessed 20 February 2018).

Polyanskiy, M.N., 2017. Refractive index database. https://refractiveindex.info. (Accessed 3 April 2017).

Swatowska, B., et al., 2011. The role of antireflective coatings in silicon solar cells –the influence on their electrical parameters. Opt. Appl. 2, 487–492.

Zoolfakar, et al. 2009. Characterization of single and dual layer anti reflecting coating (ARC) for solar cell applications. In: IEEE Conference on Information and Multimedia Technology, ICIMT '09. Jeju Island, South Korea, pp. 543–547.